Macromolecules

ARTICLE

pubs.acs.org/Macromolecules

Effects of Reactive Annealing on the Structure of Poly(methacrylic acid)−Poly(methyl methacrylate) Diblock Copolymer Thin Films

Yan Sun,[†,‡] Kevin J. Henderson,[†] Zhang Jiang,[‡] Joseph W. Strzalka,[‡] Jin Wang,[‡] and Kenneth R. Shull*[,†]

[†]Department of Materials Science and Engineering, Northwestern University, Evanston, Illinois 60208, United States

[‡]Advanced Photon Source, Argonne National Laboratory, Argonne, Illinois 60439, United States

ABSTRACT: We monitor the structural evolution of a poly(*tert*-butyl methacrylate)-poly(methyl methacrylate) (P*t*BMA−PMMA) diblock copolymer thin film undergoing conversion via reactive annealing to yield poly(methacrylic acid)−poly(methyl methacrylate) (PMAA−PMMA). Using grazing-incidence small-angle X-ray scattering (GISAXS) and atomic force microscopy (AFM), we confirm the generation of well-ordered cylindrical microdomains in the P*t*BMA−PMMA precursor film after solvent annealing. After initiating thermal deprotection, the high degree of ordering can be maintained up to 25% conversion of the diblock into PMAA−PMMA. Beyond this point, a significant decrease in the overall film thickness associated with the conversion process cannot accommodate the hexagonal lattice adopted by the cylindrical microdomains. At the same time, rearrangement of PMMA cores in a P*t*BMA matrix that is becoming progressively glassier presents further difficulties in maintaining a reasonable structure. The fully converted PMAA−PMMA film contains a system of cylindrical microdomains that lack good ordering.

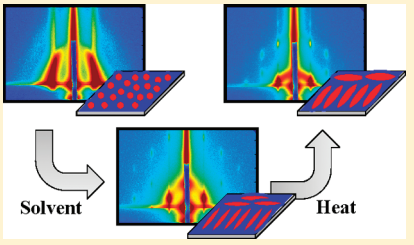

1. INTRODUCTION

Block copolymer thin films have been well exploited for their generation of highly ordered nanostructures, which are necessary for a myriad of nanopatterning and lithographic applications. The self-assembly process is governed by a combination of thermodynamic and kinetic contributions, posing a variety of challenges from a fabrication and processing standpoint. The morphologies adopted by a block copolymer film are dependent on a host of adjustable parameters, including the chemical composition and relative lengths of the blocks, interaction strength between the blocks, film thickness, substrate chemistry and patterning, and surface and interfacial energies.[1−5] In addition, effects from extra components involved in processing a film, such as a small-molecule solvent, often need to be taken into account.[6,7] A final complication, which is the focus of this paper, concerns the *in situ* modification of the chemistry of the block copolymer itself, where its composition evolves with time during processing.[8]

The block copolymer of interest in this study is a diblock copolymer consisting of a hydrophobic block connected to a longer second block that can undergo conversion from a hydrophobic polymer to a hydrophilic one during processing. Films of these resulting amphiphilic block copolymers are an attractive class of materials offering a foundation for numerous industrial and biomedical applications in aqueous environments. Their responsive behavior (toward pH or ions) and reactive functionalities (i.e., COOH) provide the opportunity for developing sophisticated filtration technology and vehicles for drug delivery.[9,10] Direct preparation and processing of amphiphilic copolymer films such as poly(styrene)−poly(acrylic acid) (PS−PAA) to generate nanopatterns and ordered morphologies have traditionally been more challenging than the more versatile and manageable hydrophobic ones such as poly(styrene)−poly(methyl methacrylate) (PS−PMMA).[11−14] Because of the large solubility differences between the blocks of amphiphilic copolymers in water, organics, and a variety of other solvents, solvent casting usually results in films comprised of spherical microdomains that are kinetically trapped and are extremely difficult to manipulate any further. PS−PAA is a diblock that has been thoroughly investigated in solution since the mid-1990s.[15] Because of the formation of reverse micelles in most organic solvents, PS−PAA was at first only studied in colloidal assemblies spun cast from toluene.[16] Consequently, the ester linkage in poly(*tert*-butyl acrylate) (P*t*BA) was advantageously employed in thin films of the nonamphiphilic PS−P*t*BA[17−21] to convert the P*t*BA block into PAA via thermal or acid-catalyzed deprotection.[22] This same procedure has also been used in an ABC-type triblock copolymer to generate water-swollen perforated lamellar structures composed of poly(styrene)-poly(vinylpyridine)-poly(*tert*-butyl methacrylate) (PS−PVP−P*t*BMA).[23] Such an *in situ* conversion process has made copolymers such as PS−PAA more accessible in terms of available thin film morphologies and has contributed to their success in the generation of responsive surfaces,[18,19] cavitated nanoreactors,[16,24] and templates for forming inorganic nanostructures.[17,25,26]

The structural evolution of these block copolymer films during annealing where one of the blocks, P*t*BA or P*t*BMA, undergoes *in situ* conversion to PAA or poly(methacrylic acid) (PMAA), is a complex yet intriguing process where ordering and arrangement in the film can be directly dictated by alterations in the chemical

Received: May 2, 2011
Revised: July 12, 2011
Published: July 22, 2011

ACS Publications © 2011 American Chemical Society

identity and interactions of the blocks, glass transition temperature, film density and thickness, and numerous other factors. In the study by La et al. involving fabrication methods for nanodots,[17] the conversion of PS−P*t*BA diblock films to PS−PAA via thermal deprotection was accompanied by a transition of well-ordered cylindrical microdomains to spherical ones due to a change in the volume fraction of the converting block. Here, annealing was easily conducted above the glass transition temperatures of both the P*t*BA (T_g = 49 °C)[27] and PAA (T_g = 106 °C)[28] so that the diblock always remained kinetically mobile for morphological arrangement throughout the conversion process. In the case of P*t*BMA (T_g = 111 °C)[29] converting to PMAA (T_g = 228 °C),[30] sample equilibration by thermal annealing cannot be accomplished because anhydride formation and depolymerization occur at temperatures approaching T_g for PMAA.[30,31] Thermal annealing above T_g for the unconverted P*t*BMA is still possible, but one must account for the continuous increase in T_g during conversion, leading to kinetic trapping of microdomains in a matrix that is becoming progressively glassier. In this paper, we focus on monitoring the ability for a P*t*BMA−PMMA diblock film to provide ordered nanostructures during an *in situ* thermal deprotection process to yield PMAA−PMMA. We show that such a state may be attained with a considerable amount of P*t*BMA conversion, although once the system achieves full conversion, the structure is found to be kinetically frozen in a less ordered state. While, for practical purposes, acid-catalyzed deprotection could be a better alternative in this case,[22,32,33] the intent of this study is to demonstrate an important pitfall which may be encountered during such an *in situ* chemical modification procedure for block copolymer films similar to this one.

Thermal deprotection of the precursor P*t*BMA−PMMA diblock film to generate PMAA−PMMA involves cleaving off the *tert*-butyl functionality in P*t*BMA, as presented in Figure 1. An annealing temperature between 160 and 200 °C provides reasonable time scales for the conversion (hours to a few days), though at these temperatures, the possibility of some anhydride formation cannot be ruled out.[31] The complete annealing procedure we have performed in this study is illustrated in Figure 2. A solution of the precursor P*t*BMA−PMMA diblock is initially prepared in a selective solvent for P*t*BMA. Spin coating of this solution forms a micellar film that serves as a well-defined

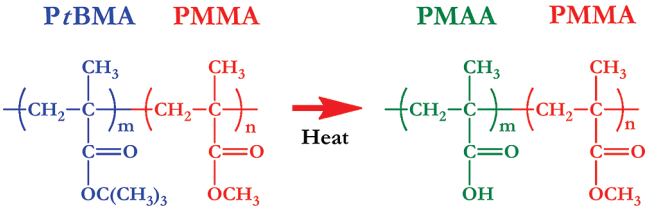

Figure 1. Chemical structures of the P*t*BMA−PMMA and PMAA−PMMA diblock copolymers. The *tert*-butyl functionality of P*t*BMA can be cleaved off to generate PMAA via thermal deprotection.

starting point for studying the morphological progression during subsequent processing stages.[34] A major step in our processing scheme involves solvent annealing of the P*t*BMA−PMMA film prior to thermal annealing in order to generate an array of well-ordered nanostructures, in this case cylinders, to be carried through the conversion process that follows. Without this crucial step (that is, if thermal deprotection were carried out on the P*t*BMA−PMMA film directly after spin coating), the system of spun-cast spherical microdomains would be too kinetically slow for major structural organization compared to the rate of conversion, freezing in the morphology too soon. Solvent annealing of a fully converted PMAA−PMMA film also presents difficulties due to the very limited selection of suitable volatile solvents that can mobilize both blocks.[9] The solvent annealing step shown in Figure 2 enhances the ability of the system to move toward achieving a morphology that is more representative of the equilibrated state. In this work, a combination of thermogravimetric analysis (TGA), atomic force microscopy (AFM), X-ray reflectivity, and grazing-incidence small-angle X-ray scattering (GISAXS) performed *in situ* reveals a complete picture of the effects that the thermal deprotection process has on the structural evolution of a P*t*BMA-containing diblock copolymer film.

2. EXPERIMENTAL SECTION

2.1. Materials. The precursor diblock copolymer poly(*tert*-butyl methacrylate)−poly(methyl methacrylate) (P*t*BMA−PMMA) was synthesized via anionic polymerization as given in a previous paper.[9] Using gel-permeation chromatography, we determined the molecular weights of the P*t*BMA and PMMA blocks to be 22.5 kg/mol and 11.0 kg/mol, respectively, with a polydispersity index of 1.07, resulting in a PMMA volume fraction of ∼0.3. The diblock was dissolved in 1-butanol at 80 °C to make solutions of up to 5 wt % and cooled through the critical micelle temperature down to room temperature prior to spin coating. Because of the presence of solvent, swollen spherical micelles of the diblock with PMMA as the cores were initially obtained in the alcohol solution.[34,35] The spherical morphology is retained during solvent drying because of the glassy natures of the swollen PMMA cores.

Samples for AFM and the X-ray experiments were prepared on cut pieces of 1 mm-thick silicon wafers (Silicon Quest International) with a thin native oxide layer (∼1 to 2 nm) and rinsed with deionized water, acetone, and methanol before being subjected to ultraviolet/ozone cleaning (UVO Cleaner Model 42, Jelight Co.) for 20 min. A spin coater from Headway Research, Inc. (Model 1-EC101-CB15) was used to deposit the diblock onto the silicon substrates. After spin coating from butanol at 3000 rpm for 30 s, we obtained film thicknesses from several tens of nanometers up to ∼150 nm (as measured with an ellipsometer, M-2000D, J.A. Woollam Co., Inc.) depending on the solution concentration.

Two types of annealing treatments were carried out in this study. Solvent annealing was conducted at room temperature by placing the sample alongside a tetrahydrofuran (THF) solvent bath inside a well-sealed

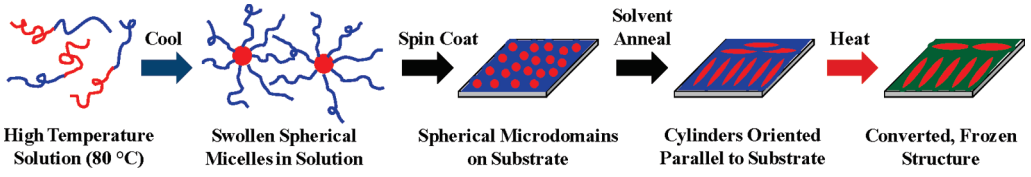

Figure 2. Illustration showing the complete annealing procedure undertaken in this study for generating nanostructures in a PMAA−PMMA film from a P*t*BMA−PMMA (22.5k-11.0k) precursor diblock. Red, blue, and green colors represent PMMA, P*t*BMA, and PMAA, respectively.

dx.doi.org/10.1021/ma201000g |*Macromolecules* 2011, 44, 6525–6531

container to ensure the solvent vapor was able to plasticize the polymer film effectively. The vapor pressure of the THF was controlled by mixing with nonvolatile 2-ethyl-1-hexanol (2EH) at a 90/10 molar ratio, yielding an estimated vapor pressure of 130 Torr at 20 °C. Thermal annealing was performed in a standard laboratory oven under vacuum at 160 and 180 °C. For the *in situ* GISAXS measurements, both thermal and solvent annealing utilized a sealed chamber with polyimide windows penetrable by X-rays. Here, the temperature of the sample was controlled by a Peltier heater as well as by a heated copper block positioned underneath the chamber. During this procedure, the interior of the chamber was placed under nitrogen to minimize beam damage to the polymer film.

2.2. Methods. Four experimental techniques were employed in this work to investigate the structural evolution of the diblock system. TGA was used to determine the temperature-dependent rate at which P*t*BMA−PMMA converted to PMAA−PMMA through the weight loss that occurred during heating. This information served as a guide for understanding our X-ray structural measurements during various stages of annealing. X-ray reflectivity provided measurements of the film thickness as well as electron density via the polymer critical angle. GISAXS patterns collected at various grazing incident angles over macroscopically large areas of the sample were used to monitor changes in the microdomain spacing and overall extent of the nanostructure ordering with high accuracy. Finally, AFM characterization provided a complementary real-space confirmation of the morphology on the sample surface.

Thermogravimetric analysis was performed using a Mettler Toledo Thermogravimetric Analyzer (model TGA/SDTA851^e) on bulk P*t*BMA−PMMA samples with initial weights of 3 to 5 mg in a nitrogen environment. The weight of the dry polymer powders was monitored over time as they were isothermally heated at 160 and 180 °C. AFM measurements were conducted in noncontact mode in air at room temperature using a high-resolution scanning probe microscope (JEOL JSPM-5200). We utilized a standard silicon probe of pyramidal shape, a tip radius of less than 10 nm, and a tip height of 14 to 16 μm (ACTA, Applied NanoStructures, Inc.). Both topography and phase images were captured, but only the phase images were able to reveal the boundaries and packing of the micelles with the necessary clarity.

Both GISAXS and X-ray reflectivity are well-known, powerful techniques capable of characterizing the nanostructure and thickness of thin films averaged over long distances.[36,37] The experiments were performed with synchrotron radiation on the 8-ID beamline at the Advanced Photon Source at Argonne National Laboratory. The standard configuration involved an X-ray energy of 7.35 keV (λ = 0.169 nm) and a beam size of 0.1 mm wide and 0.05 mm high before impinging on the sample. An avalanche photodiode detector was used for sample alignment and the reflectivity measurements, while a MAR165 CCD (or PILATUS 1 M pixel array) detector captured the two-dimensional GISAXS patterns with a pixel size of 79 (or 172) μm. The distance between the sample and the area detector, which was calibrated with a silver behenate standard, was close to 2 m. A lead beam stop was also placed in front of the detector to block the intense specular beam. GISAXS patterns were collected at several incident angles, which determined the penetration depth of X-rays into the film and thus the region from which data was collected. We focused on obtaining patterns from right below and above the critical angle of the film, corresponding to information originating from the surface and interior of the film, respectively.[38] The GISAXS patterns were saved as 2048 × 2048 16-bit TIFF images (for the case of MAR165) and processed with a beamline MATLAB program (which took into account the sample-to-detector distance and detector resolution) to produce intensity maps in the q_y−q_z plane, where q_y is the scattering vector component parallel to the sample surface and perpendicular to the scattering plane and q_z is the component perpendicular to the sample surface.

The thickness of the diblock films were extracted from fitting the reflectivity data according to Parratt's recursion formulation[39] via χ^2-minimization (Levenberg−Marquardt method). The microdomain spacing was obtained by taking line scans of GISAXS patterns in q_y at a fixed q_z and measuring the q_y position of the first-order peak using a Gaussian fit. For samples that exhibited higher-order peaks, the physical arrangement or packing geometry of the microdomains was determined by matching the positions of the diffraction peaks on the GISAXS patterns to theoretically calculated positions from an assumed lattice structure. Our choice for this assumed structure was based on the AFM images and the arrangement of the empirical peaks in the q_y−q_z plane, which were expected to translate into a similar arrangement of microdomains in real space. The simulated peak positions were calculated using the theory of the distorted-wave Born approximation (DWBA), as described in detail in previous papers.[38,40−43] Specifically, we followed the procedure of Stein et al. to generate an array of diffraction coordinates which we overlaid with our GISAXS patterns.[38] Changes in the corresponding lattice constants revealed the structural evolution of the diblocks in each annealing step. We describe this analysis in more detail in the next section.

3. RESULTS AND DISCUSSION

3.1. Kinetics of the P*t*BMA-to-PMAA Conversion. Obtaining an accurate measurement of the rate at which P*t*BMA−PMMA converts to PMAA−PMMA via thermal deprotection is essential for analyzing and understanding the observed structural changes in our films. In the next two subsections, we quantify precisely the conversion kinetics of the diblock, comparing the behavior in the bulk and in thin films. We confirm that the conversion behavior is identical in both cases, allowing us to consider bulk properties when analyzing the results for our thin films.

3.1.1. Reaction Kinetics in the Bulk Material. Measurement of the chemical conversion of a polymer in the bulk and in thin films can be readily performed with a variety of available approaches. Wallraff et al. have previously reported on the kinetics of the conversion for a P*t*BMA homopolymer in the range of 180 to 220 °C.[22] The results from these isothermal heating experiments suggested a two-step process involving an induction period (slow conversion rate) followed by a gradual transition to an autoaccelerated mechanism (faster conversion rate) where converted PMAA facilitates the further production of PMAA from P*t*BMA. Accordingly, a reaction scheme given by (1) P*t*BMA → PMAA and (2) P*t*BMA + *n*PMAA → (*n* + 1)PMAA was used in a stochastic simulation of chemical kinetics to determine the rate constants for this multistep reaction mechanism. In our study, we performed isothermal heating on our specific P*t*BMA−PMMA diblock using TGA. The weight of the bulk diblock was monitored as a function of time at 160 and 180 °C until it approached some constant value, indicating that conversion of the P*t*BMA block was complete. In both cases, a final weight loss of ∼28% was observed, which is reasonably close to the value of 26.5% that is predicted by stoichiometry if anhydride formation is assumed not to occur. The discrepancy can likely be attributed to the loss of water and thus the formation of some poly(methacrylic anhydride). Similar TGA measurements performed on a PMMA homopolymer revealed no weight loss, indicating that the PMMA block should not have been chemically altered by the heating. Figure 3 plots the fraction of P*t*BMA units remaining in the system as a function of annealing time. As can be directly observed, the conversion of the P*t*BMA block is initially slow but later speeds up, which is consistent with the mechanism proposed

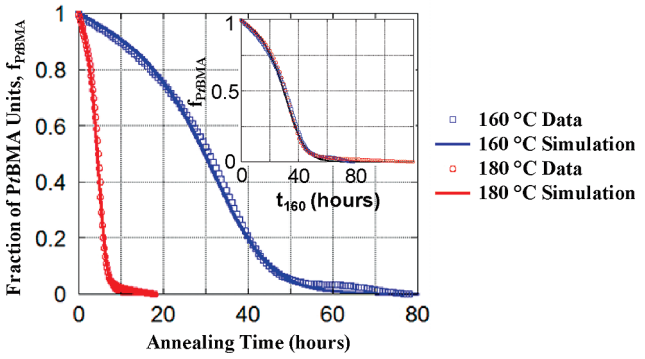

Figure 3. TGA data showing the fraction of unconverted P*t*BMA units versus annealing time for the P*t*BMA−PMMA diblock at 160 and 180 °C. The solid lines are simulated curves based on chemical kinetics calculations. The inset shows the master curve obtained from time−temperature superposition using a reference temperature of 160 °C.

by Wallraff et al. A theoretical calculation with the same reaction scheme as above was performed using the *Chemical Kinetics Simulator* program from IBM Research−Almaden.[44,45] Input parameters included the rate constants for each reaction step, which comprise an activation energy E_a in addition to a pre-exponential factor. Here, the parameters from Wallraff et al. were used as a starting point and the simulated curves were carefully matched to our experimental data through fine adjustments of the values.[22] The best fit to our data gave E_a = 40.9 kcal/mol for the first reaction and E_a = 37.9 kcal/*mol* for the second reaction, with n = 1.5. The simulated curves for 160 and 180 °C are shown with the TGA data in Figure 3. As a further step, the data at our two temperatures can be merged into a single master curve following the time−temperature superposition principle, using a reference temperature of 160 °C (433 K) in this case. The inset of Figure 3 plots the shifted TGA data with the horizontal time axis t_{160} defined as

$$t_{160} = \int_0^t \exp\left[-\frac{E_a}{R}\left(\frac{1}{T(t)} - \frac{1}{433K}\right)\right] dt \qquad (1)$$

where t is the original annealing time, T is the absolute temperature at which the TGA data is collected, E_a is the activation energy, and R is the universal gas constant. Through this method, we obtain for E_a a single value of 37.5 kcal/mol, which is quite close to the result obtained for the second reaction (autoacceleration step) in the chemical kinetics simulation above. This master curve is utilized in the next subsection for comparing the bulk kinetics to the physical changes observable in our P*t*BMA−PMMA films during thermal annealing.

3.1.2. Reaction Kinetics in Thin Films. For our P*t*BMA−PMMA diblock films, the thermal deprotection process is expected to have a significant impact on the overall film thickness and electron density, which, in turn, can affect the ordering of nanostructures inside the films. The *tert*-butyl group on the P*t*BMA is removed during conversion to form PMAA, which has a higher known bulk density (1.29 g/cm^3) than P*t*BMA (1.02 g/cm^3). X-ray reflectivity was employed to obtain the film thickness and electron density for a variety of samples. Figure 4a presents two examples of reflectivity curves and their corresponding fits for a P*t*BMA−PMMA film as spun cast and thermally annealed for 72 h at 160 °C, which is essentially a fully converted PMAA−PMMA film. The number of fringes is clearly reduced

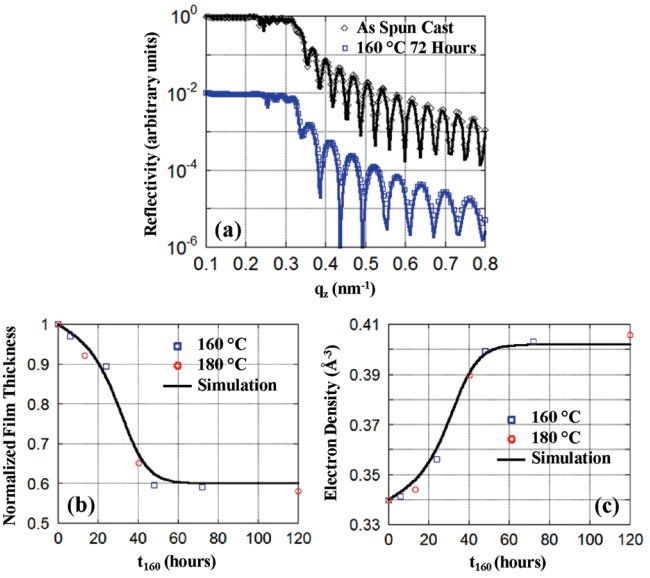

Figure 4. (a) Reflectivity data near $\theta_{c,film}$ for a P*t*BMA−PMMA film as spun cast and thermally annealed at 160 °C for 72 h. The solid lines are fits to the data. The curves are shifted vertically for clarity. (b) Plot of normalized film thickness versus shifted annealing time t_{160}, which forms a master curve with a reference temperature of 160 °C. (c) Plot of electron density of the film versus shifted annealing time t_{160}. The solid lines in parts b and c correspond to kinetic predictions obtained from the TGA data of a bulk sample.

after the annealing process, which through fitting corresponds to a thickness change from ∼154 nm to ∼96 nm, a decrease of roughly 38%. Measurements were also performed on films with other initial thicknesses, and we find that all of them generally undergo a decrease of ∼40% in thickness after full conversion. Comparing with an expected decrease of 36.4% from stoichiometric predictions with a density change considered, we can again attribute this small difference to some anhydride formation. We also collected the reflectivity at various time points during thermal annealing at 160 and 180 °C. Figure 4b plots the evolution in the film thickness, normalized by the initial thickness, as a function of the shifted annealing time t_{160}. Additionally, the master curve in Figure 3 obtained from TGA is rescaled and shown with the data. A remarkable agreement can be seen between the film thickness and conversion behavior, which confirms our expectations. The reflectivity curves also furnish information about the electron density of the film via measurement of the polymer critical angle $\theta_{c,film}$. Through fitting of our data, $\theta_{c,film}$ is seen to increase from ∼0.17 to 0.18 degrees (q_z ∼0.22 to 0.24 nm^{-1}) during the course of the conversion, corresponding to an electron density increase from ∼0.34 to 0.40 electrons/Å^3. These values translate into a density of ∼1.04 g/cm^3 for the unconverted P*t*BMA−PMMA film and ∼1.24 g/cm^3 for the fully converted PMAA−PMMA film, which match well with predictions obtained from a weighted average (using weight fractions) of the known bulk density values for the polymer blocks. Figure 4c plots the evolution in the electron density of the film as a function of t_{160}. Again, the TGA master curve in Figure 3 is shown with the data, yielding an excellent agreement. This similarity means that the kinetic parameters obtained from the thermogravimetric analysis of the bulk polymer samples can be used to quantify the conversion state of the thin films as well.

dx.doi.org/10.1021/ma201000g |*Macromolecules* 2011, 44, 6525–6531

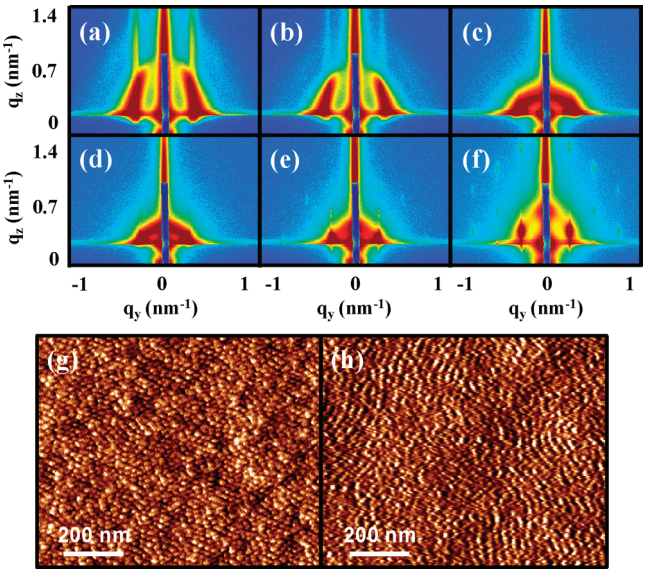

Figure 5. GISAXS patterns ($\theta_i = 1.03\theta_{c,film}$) of a P*t*BMA−PMMA film (a) as spun cast, during solvent annealing in a 90/10 THF/2EH mixture at room temperature for (b) 10 min, (c) 30 min, (d) 1 h, (e) 2 h, and (f) after solvent removal. Also shown are AFM phase images of the film surface (g) as spun cast and (h) after solvent annealing for 2 h and solvent removal.

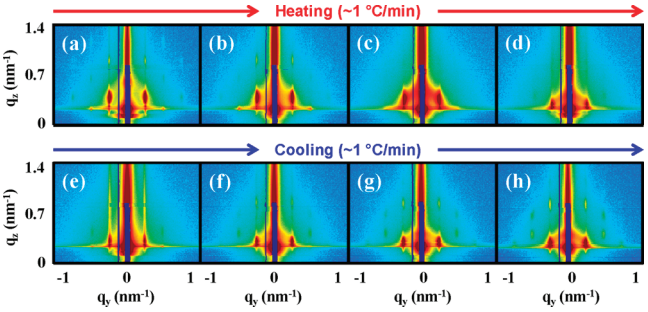

Figure 6. GISAXS patterns ($\theta_i = 1.03\theta_{c,film}$) of a solvent annealed P*t*BMA−PMMA film undergoing thermal annealing. Data from the heating phase were taken at (a) 120 °C, (b) 133 °C, (c) 145 °C, and (d) 157 °C. After annealing for 4 h at 160 °C, data were taken during cooling at (e) 157 °C, (f) 133 °C, (g) 121 °C, and (h) 111 °C. Heating and cooling rates were ~1 °C/min.

3.2. Structural Development During Processing. As discussed earlier, the precursor P*t*BMA−PMMA film produced by spin coating from the butanol solution consists of spherical microdomains. However, based on self-consistent field theory calculations of diblock melts, a cylindrical microdomain morphology is more appropriate for the PMMA volume fraction of ~0.3 in the unconverted polymer,[46] so the system of spheres is expected to evolve toward one with cylinders, even in the absence of conversion of the P*t*BMA to PMAA. The fully converted polymer has an even higher PMMA volume fraction of ~0.47, where the initial spherical morphology is even more unfavorable. In the next three subsections, we explore the evolution of nanostructures in the diblock films during solvent annealing at room temperature and during subsequent thermal annealing for two different scenarios: Annealing for a short time prior to thermal conversion and annealing for a long time during which thermal conversion is fully underway. We show that these morphological changes are consistent with these very general thermodynamic considerations.

3.2.1. Structural Development During Solvent Annealing. As indicated previously in Figure 2, the first step in processing our precursor P*t*BMA−PMMA films is performing solvent annealing in order to plasticize the material and generate ordered morphologies prior to starting the thermal deprotection process. For this diblock, volatile organics such as THF can work effectively to mobilize both blocks, though exposing the sample for too long to pure THF vapor (more than ~1 to 2 h) may completely disorder the nanostructure. Therefore, 90/10 molar ratio mixtures of THF and 2EH were used to control the THF vapor pressure for solvent annealing. *In situ* GISAXS measurements were conducted to monitor the structure of the film during the annealing process at room temperature for up to 2 h. Figure 5a-f shows a series of patterns taken with the incident X-ray angle slightly above the polymer critical angle ($\theta_i = 1.03\theta_{c,film}$), providing information from the entire extent of the film. As expected, the as-spun cast morphology according to Figure 5a consists of spherical microdomains that lack good ordering. A well-defined layer of microdomains at the surface of the film contributes to a set of long vertical rods observed in the pattern (also seen more prominently in a pattern taken below the polymer critical angle, $\theta_i < \theta_{c,film}$), while a semicircular ring (seen only for $\theta_i > \theta_{c,film}$) corresponds to partially ordered microdomains in the interior of the film. Analysis of the first-order peak from a horizontal line scan in q_y reveals that the spacing between microdomains in this nonequilibrium state is around 19.0 nm. Figure 5g is an AFM phase image of the as-spun cast surface and confirms this observation. As the film is being solvent annealed (Figure 5b−d), we see the vertical rods quickly start to disappear and the semicircular ring collapses, corresponding to significant disordering of the as-spun cast structure both at the surface and in the interior of the film. Because of solvent uptake, the spacing between the disordered microdomains increases along with the entire film thickness, swelling by ~68% according to *in situ* reflectivity measurements. After 2 h of solvent annealing, individual diffraction spots start to appear as seen in Figure 5e, signifying the creation of an array of cylindrical microdomains lying parallel to the substrate in a hexagonally packed fashion. Finally, upon fast removal of the solvent from the film (by opening the annealing chamber), the diffraction spots are shifted upward as seen in Figure 5f, corresponding to a collapse of the cylinders in the vertical direction in real space. In the horizontal direction, the cylinders are pinned by the substrate and alter little. Therefore, the lattice after drying is a distorted hexagonal lattice (or centered rectangular lattice). From a simulation of peak positions as depicted in Figure 7a, the exact lattice constants are determined to be $a = 24.8$ nm (horizontal direction) and $c = 28.8$ nm (vertical direction) as defined on the diagram in the figure, translating to a distortion of 33% relative to a perfect hexagonal lattice. From the full width at half-maximum (fwhm) of the peaks in the horizontal direction, we estimate a grain size, $d = 2\pi/\text{fwhm}$, of around ~300 nm, corresponding to roughly 12 cylinders in-plane. We must note that a GISAXS pattern taken with $\theta_i < \theta_{c,film}$ does not exhibit any high-order diffraction spots. Appropriately, Figure 5h is an AFM phase image of the solvent annealed and dried P*t*BMA−PMMA film, showing the indication of only short parallel cylinders on the surface. On the basis of the fact that high-order diffraction spots appear in our GISAXS patterns only for $\theta_i > \theta_{c,film}$, we suspect that the parallel microdomains are more highly ordered in the bulk of the film than at the surface.

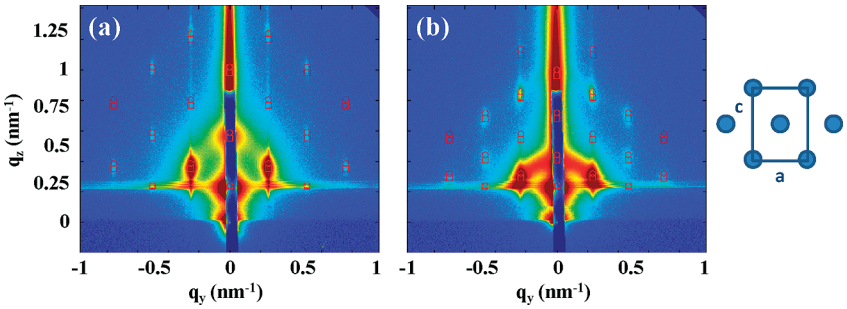

Figure 7. GISAXS patterns ($\theta_i = 1.03\theta_{c,film}$) of (a) dried P*t*BMA−PMMA film after solvent annealing in a 90/10 THF/2EH mixture for 2 h and (b) after subsequent thermal annealing at 160 °C for 4 h. Red circles and squares correspond to simulated diffraction peaks due to the reflected and transmitted beams, respectively. The patterns correspond to cylinders stacked parallel to the substrate. The packing motif is that of a centered rectangular lattice distorted in the film thickness direction (see schematic). The lattice constants are (a) a = 24.8 nm and c = 28.8 nm and (b) a = 26.9 nm and c = 44.3 nm.

3.2.2. Structural Development During Thermal Annealing Prior to Reaction. After applying solvent annealing to induce ordered morphologies in our precursor P*t*BMA−PMMA films, thermal annealing was performed to convert the films to PMAA−PMMA. Our TGA results estimate that an annealing time of at least 72 h at 160 °C or 18 h at 180 °C is required for full conversion. First, in order to understand how the structure of the films can evolve prior to the conversion of the P*t*BMA blocks to PMAA, we performed GISAXS measurements at elevated temperatures but for times short enough so that the conversion remains below 1%. Figure 6 shows a series of GISAXS patterns of a P*t*BMA−PMMA film taken during heating as well as during cooling after a 4-h hold at 160 °C. The heating and cooling rates were ∼1 °C per minute, but data were always collected at fixed temperatures that were stabilized for ∼10 min during the heating or cooling process. Here, we see that the diffraction spots obtained after solvent annealing can be retained up to a temperature of ∼120 °C, which is around the glass transition temperature of both polymer blocks (Figure 6a). Beyond this temperature, all spots except the first-order peak disappear as seen in Figure 6b,c, indicating the loss of good ordering of the microdomains. A noticeable shift in the position of the first-order peak toward smaller q_z is seen upon reaching ∼160 °C (Figure 6d), indicating that a new, larger microdomain spacing has formed. From a simulation of peak positions as depicted in Figure 7b, the exact lattice constants are determined to be a = 26.9 nm (horizontal direction) and c = 44.3 nm (vertical direction) as defined on the diagram in the figure, translating to a distortion of now only 5% relative to a perfect hexagonal lattice.

3.2.3. Structural Development During Thermal Annealing with Reaction. The question now regards whether the hexagonally packed cylindrical microdomains with the high degree of ordering obtained in the previous section can be retained with a much longer thermal annealing treatment, enough for conversion of the diblock into PMAA−PMMA. An obvious concern is the inevitable decreasing film thickness associated with the thermal deprotection process as the reflectivity analysis has shown. Additionally, both the P*t*BMA matrix and PMMA cores are sufficiently mobile for some reorganization to occur before the matrix is immobilized by the conversion to PMAA. Although a change in the relative volume fractions of the two polymer blocks is expected during conversion, ultimately favoring more of a lamellar morphology at equilibrium rather than cylinders, the system appears to remain kinetically trapped in a poorly ordered cylindrical morphology. Figure 8 shows GISAXS patterns of the

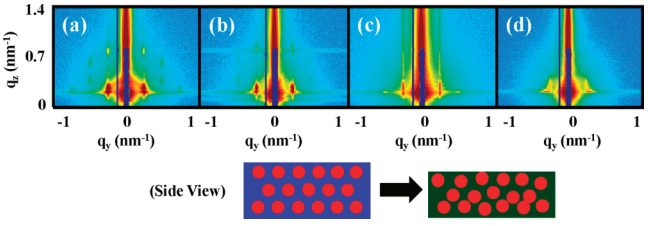

Figure 8. GISAXS patterns ($\theta_i = 1.03\theta_{c,film}$) of a solvent annealed P*t*BMA−PMMA film after thermal annealing at 160 °C for (a) 6 h, (b) 24 h, (c) 48 h, and (d) 72 h. The data were collected at room temperature. The corresponding percentage conversions of the film into PMAA−PMMA are approximately (a) 3%, (b) 25%, (c) 89%, and (d) 99%. Also shown is an illustration (side view) depicting the structural changes in the film during the thermal deprotection procedure.

diblock taken at room temperature after thermal annealing at 160 °C for 6, 24, 48, and 72 h. As can be seen in Figure 8a and b, the series of diffraction spots identical to the one in Figure 6h can be easily retained up to at least 24 h of annealing at 160 °C, corresponding to a percent conversion to PMAA−PMMA of ∼25%. The PMMA volume fraction at ∼25% conversion is calculated to be around ∼0.33, which still places the system in the cylindrical regime. The glass transition temperature of the partially converted matrix here is estimated to be around 140 °C (based on a weighted average of the T_g values of P*t*BMA and PMAA), suggesting that polymer mobility is not yet of concern. The pattern in Figure 8c after 48 h of annealing (∼89% conversion) appears qualitatively very similar to the one taken *in situ* at an elevated temperature in Figure 6e. At this point, the corresponding film thickness is decreased by almost ∼40% based on reflectivity measurements and the PMMA volume fraction should increase to ∼0.44, placing the system in the lamellar regime. However, the T_g of the matrix is now estimated to be around 215 °C, which is well above the annealing temperature of 160 °C. The absence of high-order diffraction spots implies the packing geometry has been physically perturbed enough to deviate from a perfect hexagonal lattice, where the now kinetically frozen cylindrical microdomains no longer possess a high degree of ordering. Finally, after 72 h of annealing (Figure 8d), the microdomain ordering both at the surface and in the interior of the film is essentially lost due to the significantly reduced film thickness, which is clearly unable to accommodate the original lattice. Therefore, a rather disordered system of microdomains is obtained in the final fully converted PMAA−PMMA film.

dx.doi.org/10.1021/ma201000g |*Macromolecules* 2011, 44, 6525–6531

We also note that annealing the same system using a temperature of 180 °C results in almost identical behavior as that of 160 °C, with disordered microdomains obtained at the end of the conversion process. This reduction in the order of the cylindrical microdomains is very difficult to avoid in the thermal conversion process that we have used. As mentioned in the Introduction, acid-catalyzed deprotection at lower temperatures may be a better alternative for maintaining good ordering during the conversion of the *tert*-butyl methacrylate groups to methacrylic acid.[32,33]

4. CONCLUSIONS

The thermal deprotection of P*t*BMA−PMMA diblock copolymer films is a complex process that may not necessarily lead to ordered morphologies in fully converted PMAA−PMMA films. Nevertheless, we have shown that the *in situ* modification of the chemistry of the diblock offers a promising means for obtaining nanostructures that are difficult to achieve through direct processing of the final amphiphilic diblock film. Here, nonequilibrium but well-defined spherical microdomains from spin coating are transformed into cylindrical microdomains that are oriented parallel to the substrate upon solvent annealing. Our *in situ* measurements clearly capture this process as the system moves toward a more equilibrium state. During the thermal deprotection step, the high degree of packing of the cylindrical microdomains can be retained up to at least 25% conversion of the diblock to PMAA−PMMA via thermal annealing. Beyond this point, the hexagonal packing geometry of the now kinetically trapped microdomains cannot be accommodated, resulting in a loss of ordering and elimination of the hexagonal lattice.

■ AUTHOR INFORMATION

Corresponding Author

*E-mail: k-shull@northwestern.edu.

■ ACKNOWLEDGMENT

The AFM work was performed in the NIFTI facility of NU*ANCE* Center at Northwestern University. NU*ANCE* Center is supported by NSF−NSEC, NSF−MRSEC, the Keck Foundation, the State of Illinois, and Northwestern University. The TGA measurements were carried out at the Polymer Characterization Laboratory at Northwestern University. The GISAXS experiments were conducted at the Advanced Photon Source at Argonne National Laboratory. Use of the APS was supported by the U.S. Department of Energy, Office of Science, Office of Basic Energy Sciences, under Contract No. DE-AC02-06CH11357. The authors gratefully acknowledge the APS staff at 8-ID for their technical support. We also acknowledge additional support from the NSF Division of Materials Research, Grant DMR-0907384.

■ REFERENCES

(1) Lazzari, M.; Lopez-Quintela, M. A. *Adv. Mater.* **2003**, *15*, 1583.
(2) Park, C.; Yoon, J.; Thomas, E. L. *Polymer* **2003**, *44*, 6725.
(3) Segalman, R. A. *Mater. Sci. Eng. R-Rep.* **2005**, *48*, 191.
(4) Hamley, I. W. *Prog. Polym. Sci.* **2009**, *34*, 1161.
(5) Albert, J. N. L.; Epps, T. H. *Mater. Today* **2010**, *13*, 24.
(6) Bohme, M.; Kuila, B.; Schlorb, H.; Nandan, B.; Stamm, M. *Phys. Status Solidi B-Basic Solid State Phys.* **2010**, *247*, 2458.
(7) Paik, M. Y.; Bosworth, J. K.; Smilges, D. M.; Schwartz, E. L.; Andre, X.; Ober, C. K. *Macromolecules* **2010**, *43*, 4253.
(8) Krishnamoorthy, S.; Hinderling, C.; Heinzelmann, H. *Mater. Today* **2006**, *9*, 40.
(9) Guvendiren, M.; Shull, K. R. *Soft Matter* **2007**, *3*, 619.
(10) Henderson, K. J.; Zhou, T. C.; Otim, K. J.; Shull, K. R. *Macromolecules* **2010**, *43*, 6193.
(11) Xu, T.; Goldbach, J. T.; Misner, M. J.; Kim, S.; Gibaud, A.; Gang, O.; Ocko, B.; Guarini, K. W.; Black, C. T.; Hawker, C. J.; Russell, T. P. *Macromolecules* **2004**, *37*, 2972.
(12) Ryu, D. Y.; Ham, S.; Kim, E.; Jeong, U.; Hawker, C. J.; Russell, T. P. *Macromolecules* **2009**, *42*, 4902.
(13) Zucchi, I. A.; Poliani, E.; Perego, M. *Nanotechnology* **2010**, *21*, 185304.
(14) Zhang, X. H.; Yager, K. G.; Fredin, N. J.; Ro, H. W.; Jones, R. L.; Karim, A.; Douglas, J. F. *ACS Nano* **2010**, *4*, 3653.
(15) Zhang, L. F.; Eisenberg, A. *Science* **1995**, *268*, 1728.
(16) Boontongkong, Y.; Cohen, R. E. *Macromolecules* **2002**, *35*, 3647.
(17) La, Y. H.; Edwards, E. W.; Park, S. M.; Nealey, P. F. *Nano Lett.* **2005**, *5*, 1379.
(18) Xu, C.; Fu, X. F.; Fryd, M.; Xu, S.; Wayland, B. B.; Winey, K. I.; Composto, R. J. *Nano Lett.* **2006**, *6*, 282.
(19) Xu, C.; Wayland, B. B.; Fryd, M.; Winey, K. I.; Composto, R. J. *Macromolecules* **2006**, *39*, 6063.
(20) Park, D. H. *Nanotechnology* **2007**, *18*, 365303.
(21) Kelly, J. Y.; Albert, J. N. L.; Howarter, J. A.; Kang, S. H.; Stafford, C. M.; Epps, T. H.; Fasolka, M. J. *ACS Appl. Mater. Interfaces* **2010**, *2*, 3241.
(22) Wallraff, G.; Hutchinson, J.; Hinsberg, W.; Houle, F.; Seidel, P.; Johnson, R.; Oldham, W. *J. Vac. Sci. Technol. B* **1994**, *12*, 3857.
(23) Ludwigs, S.; Boker, A.; Voronov, A.; Rehse, N.; Magerle, R.; Krausch, G. *Nat. Mater.* **2003**, *2*, 744.
(24) Miller, A. C.; Bennett, R. D.; Hammond, P. T.; Irvine, D. J.; Cohen, R. E. *Macromolecules* **2008**, *41*, 1739.
(25) Jang, A. J.; Lee, S. K.; Kim, S. H. *Polymer* **2010**, *51*, 3486.
(26) Kim, S. M.; Ku, S. J.; Kim, J. B. *Nanotechnology* **2010**, *21*, 235302.
(27) Cole, D. H.; Shull, K. R.; Baldo, P.; Rehn, L. *Macromolecules* **1999**, *32*, 771.
(28) Maurer, J. J.; Eustace, D. J.; Ratcliffe, C. T. *Macromolecules* **1987**, *20*, 196.
(29) Yang, H.; Sharp, J. S. *Macromolecules* **2008**, *41*, 4811.
(30) Lai, J. H. *Macromolecules* **1984**, *17*, 1010.
(31) Grant, D. H.; Grassie, N. *Polymer* **1960**, *1*, 445.
(32) Esker, A. R.; Mengel, C.; Wegner, G. *Science* **1998**, *280*, 892.
(33) Mengel, C.; Esker, A. R.; Meyer, W. H.; Wegner, G. *Langmuir* **2002**, *18*, 6365.
(34) Shull, K. R.; Martin, E. F.; Drzal, P. L.; Hersam, M. C.; Markowitz, A.; McSwain, R. *Langmuir* **2005**, *21*, 178.
(35) Drzal, P. L.; Shull, K. R. *Macromolecules* **2003**, *36*, 2000.
(36) Muller-Buschbaum, P. *Anal. Bioanal. Chem.* **2003**, *376*, 3.
(37) Muller-Buschbaum, P. Characterization of Polymer Surfaces and Thin Films. *Prog. Colliod Polym. Sci.* **2006**, *132*, 23.
(38) Stein, G. E.; Kramer, E. J.; Li, X. F.; Wang, J. *Macromolecules* **2007**, *40*, 2453.
(39) Parratt, L. G. *Phys. Rev.* **1954**, *95*, 359.
(40) Sinha, S. K.; Sirota, E. B.; Garoff, S.; Stanley, H. B. *Phys. Rev. B* **1988**, *38*, 2297.
(41) Rauscher, M.; Salditt, T.; Spohn, H. *Phys. Rev. B* **1995**, *52*, 16855.
(42) Lee, B.; Park, I.; Yoon, J.; Park, S.; Kim, J.; Kim, K. W.; Chang, T.; Ree, M. *Macromolecules* **2005**, *38*, 4311.
(43) Busch, P.; Rauscher, M.; Smilgies, D. M.; Posselt, D.; Papadakis, C. M. *J. Appl. Crystallogr.* **2006**, *39*, 433.
(44) Bunker, D. L.; Garrett, B.; Kleindienst, T.; Long, G. S. *Combust. Flame* **1974**, *23*, 373.
(45) Gillespie, D. T. *J. Comput. Phys.* **1976**, *22*, 403.
(46) Matsen, M. W.; Bates, F. S. *Macromolecules* **1996**, *29*, 1091.